Study of the Initial Corrosion of X80 Steel in a Saturated Saline Soil Co-Contaminated with Cl^-, SO_4^{2-} and HCO_3^-

Fuli Ma[1], Ruizhen Xie[1], Pengju Han[1,2,], Xiaohong Bai[1,*]*

[1] Department of Civil Engineering, Taiyuan University of Technology, Taiyuan, 030024, P. R. China
[2] State Key Laboratory of Hydraulic Engineering Simulation and Safety, Tianjin University, Tianjin, 300350, P. R. China
[*]E-mail: 13834569544@163.com, bxhong@tyut.edu.cn

An orthogonal experimental group of saline soils with soluble salt anions (Cl^-, SO_4^{2-} and HCO_3^-) was designed by orthogonal assistant and IBM SPSS statistics 21 software. The initial dynamic potentiodynamic polarization of X80 steel embedded in different saline soils was tested using a three-electrode system. The statistical range and variance in the measurement data, the corrosion morphologies and composition of the X80 steel and the corrosion mechanism were analysed. The results show that the corrosion of X80 steel in S9 was the weakest, and the corrosion current density reached 4.9E-7. The corrosive behaviour of X80 steel in different saline soils exhibited the following order: S9<S6<S3<S4<S5<S8<S2<S7<S1. The SO_4^{2-} anions mainly affected the corrosion potential, and Cl^- and HCO_3^- mainly affected the corrosion current density. The optimal contents of Cl^-, SO_4^{2-} and HCO_3^- in sandy soil are 1, 0.3, and 0.3 mmol/100 g for the R_p, respectively. The initial corrosion of X80 steel in different saline soils was weak, and mainly exhibited local pitting. SO_4^{2-} is the most important factor affecting the initial corrosion behaviour of the X80 steel. The Cl^-, SO_4^{2-} and HCO_3^- factors were not statistically significant (P>0.05), which may be due to the level selection of the experimental factors.

1. INTRODUCTION

With the rapid development of the petroleum and transportation industries, an increasing number of pipelines are buried underground due to the limitation of available space to construct these facilities [1-3]. Owing to its high intensity and high toughness, X80 steel has the potential to be widely applied in the building of gas transmission pipelines [4-6]. However, the corrosion performance of X80 steel is a key problem for the life expectancy, especially in a soil environment. The corrosion of

X80 steel has been studied for a while. In a chloride-containing alkaline environment (0.5 M Na_2CO_3 + 1 M $NaHCO_3$ solution with two different concentrations of Cl^-, 0.02 M and 0.2 M), a superimposed AC degrades the passivity of the X80 steel, shifts the corrosion potential negatively, and increases the corrosion rate. The AC and Cl^- synergistically increase the corrosion rate greatly, and the corrosion becomes more localized [7, 8]. Zhou et al. also discovered that the corrosion rate of X80 increases and then decreases with an increase in the HCO_3^- concentration in a $NaHCO_3$ solution. In a Liaohe Oilfield simulated soil solution, the corrosion rate of X80 steel presented a similar regular pattern. Only a few minor corrosion pits appeared on the surface, and the corrosion phenomenon was not obvious [9, 10]. In a simulated acid soil solution, the tensile stress promoted the movement of dislocations, which became active points enhancing the anodic dissolution rate and promoting the formation of the corrosion product film for X80 steel [11]. In aerated solutions, hydrogen enhanced the reactivity of the passive film formed on the X80 pipeline steel and reduced the corrosion resistance and thickness of this passive layer [12]. In a near-neutral soil solution, synergistic effects of elastic stress and SRB activity enhanced the corrosion of API X80 steel. The activities of SRB initiated pits, and the applied elastic stress maintained and promoted the growth of pits [13, 14]. In the underground water of acidic soil environments, ductile cracking first occurred. The crack growth rate significantly accelerated with decreasing pH value of the solution [15]. In a Dagang simulated soil solution, the potentials of hydrogen evolution of X80 were between those of X65 and X100 [16]. In an SRB-inoculated soil simulated solution (Yingtan soil), the hydrogen permeation current density of X80 steel was three times higher than that without SRB. The presence of SRB could promote stress corrosion cracking susceptibility. In addition, the protective effect of corrosion products on X80 steel was much greater than that of a biofilm [17-19]. In an NS4 near-neutral solution (used to simulate an electrolyte trapped under a disbonded coating) with Cl^-, SO_4^{2-}, HCO_3^-, the corrosion morphology of X80 steel changed from uniform corrosion to localized corrosion with many pits as the AC density increased with the assistance of the electrochemical test [20, 21].

Corrosivity of X80 steel in a soil complex medium was also investigated. In an acidic red soil, the corrosion rate of X80 steel was approximately 0.0902 mm/a at 38 weeks under a precise electrical resistance (ER) test, but the corrosion rate decreased to 0.0226 mm/a after 5 years [22]. In acidic soil (Yingtan and Xishuangbanna), alkaline soil (Korla and Dagang), and dry sandy soil (Lhasa) in China, X80 steel presents a susceptibility to stress corrosion cracking (SCC) under exposure testing [23]. In acidic soil, there is no relationship between the locations of SCC crack initiation and pitting occurrences. In alkaline soil, the SCC cracks were mainly initiated at the bottoms of pits [24]. In clay soils (Tabasco, Clay-T) from Tabasco and Campeche, X80 steel was proved to be more susceptible to corrosion by the electrochemical evaluations [25]. In near-neutral pH soil, stress vs. strain curves showed the incidence of cracking and their dependence on the potential imposed and revealed the SCC (stress corrosion cracking) susceptibility of X80 steel even under cathodic potentials [26]. In an Fe-rich red soil, the respiratory metabolic activity of SRB during the growth period significantly promoted the corrosion process of X80 steel; therefore, SRB serves as an electron mediator in the electron transfer between Fe and iron oxide [27].

The aforementioned research methods on the corrosion of X80 steel mainly include outdoor embedding tests and rapid indoor corrosion tests, and electrochemical testing technology has been

applied to the corrosiveness study of X80 steel in soil. Soil is a special solid porous electrolyte with coexisting solid, liquid and gas phases. There are various types of soil and many factors influencing the erosion, such as water content, temperature, anions, alternating current, dissolved oxygen (DO) concentration, etc. [28-32]. Previous studies of X80 steel corrosion in soil with different anions have mainly focused on Cl^-, SO_4^{2-} and HCO_3^- anions, but the effect of these anions has not been systematically studied. Orthogonal experimental design is an approach for multifactorial and multilevel studies. The method with "uniform dispersion, neat and comparable" test point is a highly efficient, rapid and economical experimental design approach. The application of statistical analysis methods will make the study of soil erosion more convenient. In this work, an orthogonal experimental group of saline soils with soluble salt anions (Cl^-, SO_4^{2-} and HCO_3^-) was designed by orthogonal assistant and IBM SPSS statistics 21 software. The initial dynamic potentiodynamic polarization of X80 embedded in different saline soils was tested using a three-electrode system. The statistical range and variance in the measurement data, the corrosion morphologies and corrosion mechanism of the X80 steel and the composition of corrosion products were analysed.

2. EXPERIMENTAL PROCEDURE

2.1 Experimental materials and pre-treatment

The sandy soil in this test is a standard sand with a quartz (SiO_2) fraction of 99.8% (China ISO Standard Sand Co., Ltd.). The saline soil was saturated with the water content of ~15%, the contents of Cl^-, SO_4^{2-} and HCO_3^- were determined according to " Chinese Standard for Geotechnical Investigation " GB 50021-2001. The concentration of the ions was measured in mill moles of ions in 100 g of soil and three different concentration were chose for each ion (Table 1). An orthogonal test was designed according to the orthogonal table L_9 (3^4). The type of ions Cl^-, SO_4^{2-} and HCO_3^- are change factors, and the three different ions concentration (Table 1) are levels for every factor in the orthogonal test. The head of orthogonal table is shown in Table 2. The experiments were arranged by IBM SPSS statistics software to eliminate the impact of the test sequence on the test results (Table 3). Saline sandy soils with 9 different combination of ions contents were prepared according to Table 3 and Table 1. Cl^-, $SO4^{2-}$ and HCO_3^- all originate from analytical sodium salt (NaCl, Na_2SO_4 and $NaHCO_3$, respectively). Sodium salts of Cl^-, SO_4^{2-} and HCO_3^- were first dissolved in deionized water and then mixed with dry sand. The saturated saline soils with different combination of ions contents were all stored in a fresh bag for 24 h to enable adequate mixing. The saline soils will be numbered with S1, S2,… and S9, corresponding with the numbers in Table 3.

The electrolytic cell is a rubber box with an internal volume of 70.7 mm × 70.7 mm × 70.7 mm. X80 specimen with the size of 15×15×2 mm was used as working electrode. Before the test, all the X80 specimen were polished with increasing grade of sandpaper #360, #800 and #1500. Then the specimens were all ultrasonically cleaned in an acetone solution for 10 min and dried. Wax Sealing was used to protect the other side of the specimen and left a work area of 1 cm^2. The X80 specimen tested in different saline soils will be numbered with X1, X2,…, and X9, corresponding with the number of the saline soil.

Table 1. Factor level table of saline soils

Levels	$C(Cl^-)$	$C(SO_4^{2-})$	$C(HCO_3^-)$
1	1.00	0.30	0.30
2	5.00	1.00	1.00
3	8.00	2.00	2.00

Note: C is a mmol of ions in 100 g of sand soil.

Table 2. The orthogonal test header of saline soils

Factors	$C(Cl^-)$	$C(SO_4^{2-})$	$C(HCO_3^-)$	Blank
Col.	1	2	3	4

Table 3. Orthogonal test scheme of saline soils

No.	$C(Cl^-)$	$C(SO_4^{2-})$	$C(HCO_3^-)$
1	3	2	1
2	1	3	3
3	3	1	3
4	1	2	2
5	2	2	3
6	3	3	2
7	2	3	1
8	2	1	2
9	1	1	1

2.2 Testing and characterization

The polarization curve tests of X80 steel in saline soils were carried out with a CS350 electrochemical workstation (Wuhan Corrtest Instrument Co., Ltd.). The tests proceeded in a three-electrode device consisting of a reference electrode (saturated calomel electrode), an auxiliary electrode (copper) and a working electrode (X80 specimen). The height of the saline soil was compressed to ~6 cm to control the medium-dense level of the density during testing. The potentiodynamic polarization was tested in the potential range of -0.3-1 V and a scan rate of 2 mV/s. The micro-morphologies of X80 specimen were obtained using a TM3000 scanning electron microscope (SEM, Hitachi-TM 3000), and the corrosion products were analysed by an energy-dispersive spectrometer (EDS) on a Bruker Quantax combined spectrum analyser. The macro-morphologies was photographed using Canon 6D SLR cameras. The weight of the samples were measured on an electronic balance with accuracy of 0.01. All the test were taken out at room temperature (~18°C).

3. RESULTS AND DISCUSSION

3.1 Polarization results of X80 steel in saline soil

The polarization results of X80 steel in different saline soils are shown in Figure 1. No obvious passivation zone appears on the anode branch of polarization curves in those weak saline soils, which may be related to the porous structure of the sandy soils. In terms of the corrosion current density, the weakest corrosion of X80 steel occurred in S9. The strongest corrosivity is exhibited in the S1, S2 and S7, and the content of Cl⁻ is greater than that in the other saline soils. However, the content of HCO_3^- is greater in the S9, S6 and S3 with weak corrosivity. This phenomenon can be explained by the formation of a passivation film on the sample surface [33]. The content of SO_4^{2-} is greater in S5, S6, S1, S2, and S7, and their polarization curves exhibit higher self-corrosion potential than that of S9. The above results show that SO_4^{2-} mainly affects the corrosion potential, while Cl⁻ and HCO_3^- mainly affect the corrosion current density.
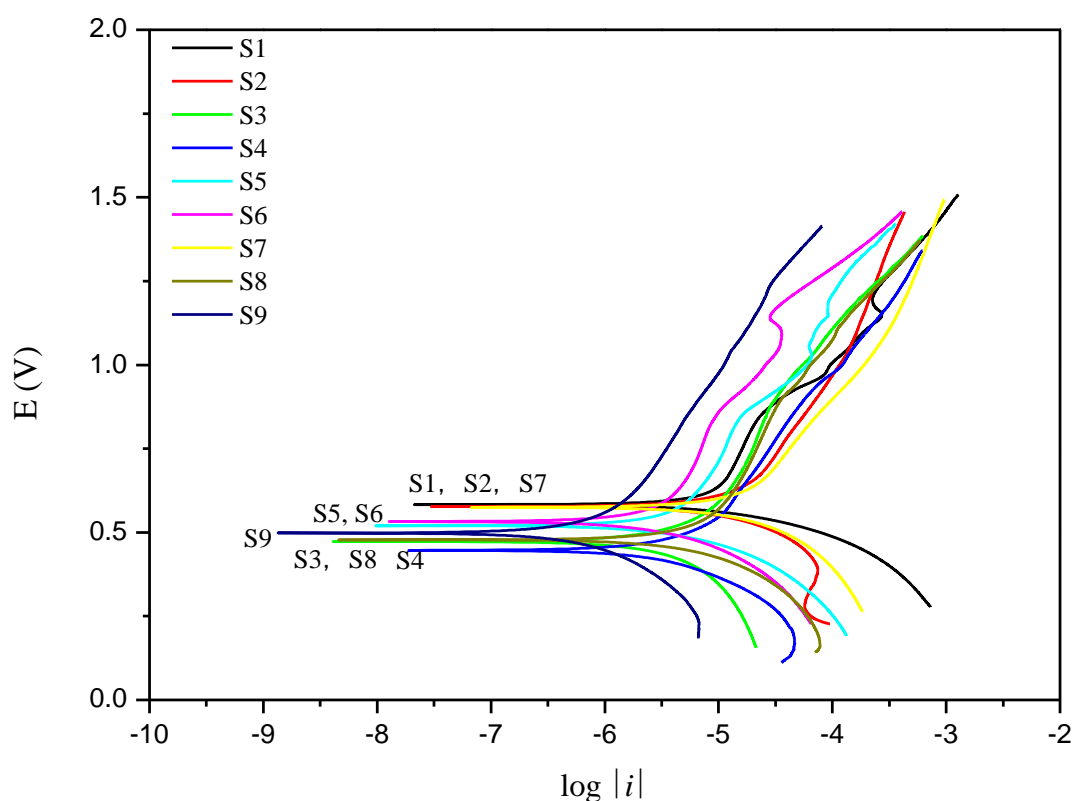
Figure 1. Polarization curves of X80 steel in saline soils under orthogonal experiment, the content of the ions (mmol) in 100 grams of soils are as following: S1: Cl⁻8.0, SO_4^{2-}1.0, HCO_3^-0.3; S2: Cl⁻1.0, SO_4^{2-}2.0 , HCO_3^-2.0; S3: Cl⁻8.0, SO_4^{2-}0.3, HCO_3^-2.0; S4: Cl⁻1.0, SO_4^{2-}1.0 , HCO_3^-1.0; S5: Cl⁻5.0, SO_4^{2-}1.0 , HCO_3^-2.0; S6: Cl⁻8.0, SO_4^{2-}2.0, HCO_3^-1.0; S7: Cl⁻5.0, SO_4^{2-}2.0, HCO_3^-0.3; S8: Cl⁻5.0, SO_4^{2-}0.3, HCO_3^-1.0; S9: Cl⁻1.0, SO_4^{2-}0.3, HCO_3^-0.3.

The weak polarization resistance (R_p) fitting results for the polarization curves are shown in Table 4, and the fitting interval is ± 50 mV (up and down the open circuit potential). The results show that the value of I_o is much less than 3 μA/cm², and a slight corrosion is exhibited [34-36]. The

corrosion of X80 steel is the weakest in S9, and I_o reached 4.9E-7. The corrosion behaviour of X80 steel in different saline soils exhibits the following order: S9<S6<S3<S4<S5<S8<S2<S7<S1. Additionally, the trend of the corrosion rate is consistent with the trend of corrosion current density.

Table 4. R_p fitting results for polarization curves of X80 steel in saline soils under orthogonal experiment

No.	E_o (V)	I_o (A/cm$^{2\sim}$)	R_p (Ω/cm$^{2\sim}$)	Corrosion rate (mm/a)
S1	0.59	1.2E-5	2275.0	0.138
S2	0.58	9.1E-6	2938.3	0.107
S3	0.47	2.4E-6	11246	0.028
S4	0.45	2.8E-6	9445.5	0.033
S5	0.53	3.5E-6	7718.7	0.041
S6	0.54	2.3E-6	11694	0.027
S7	0.58	1.1E-5	2412.8	0.130
S8	0.48	4.2E-6	6341.7	0.049
S9	0.50	4.9E-7	55043	0.006

3.2 Statistical analysis of the polarization results

3.2.1 Range analysis of the polarization results

The Orthogonal Design Assistant Ⅱ was used in the range analysis of the polarization results, and the results of the visual analysis are shown in Table 5. $I_{i,j,k}$, $II_{i,j,k}$, and $III_{i,j,k}$ are the mean values, and $R_{i,j,k}$ is the range (i, j and k represent the self-corrosion potential E_o; the polarization resistance R_p and the corrosion rates I, II, III are the three levels). It can be seen from the table that the related coefficient (R) of blank columns is larger than that of the other factors, indicating that there may be some non-negligible interactions between the factors [37].

Table 5 shows that in these weak saline soils, the influence of three factors (Cl$^-$, SO$_4^{2-}$ and HCO$_3^-$) on the E_o of X80 steel is ranked in the order of SO$_4^{2-}$> HCO$_3^-$> Cl$^-$; the influence on the R_p of X80 steel is ranked SO$_4^{2-}$> Cl$^-$ > HCO$_3^-$; and the influence on the corrosion rate of X80 steel is ranked SO$_4^{2-}$> HCO$_3^-$> Cl$^-$. In conclusion, SO$_4^{2-}$ is the most important factor affecting the initial corrosion behaviour of X80 steel due to its strong adsorption and desorption effects in weak saline soils contaminated by three anions (Cl$^-$, SO$_4^{2-}$ and HCO$_3^-$) [38, 39]. In 500 g of sand soil, the optimal solutions of Cl$^-$, SO$_4^{2-}$ and HCO$_3^-$ are 8, 2, and 0.3 mmol/100 g for the self-corrosion potential; the optimal solution is 1, 0.3, and 1 mmol/100 g for the corrosion rate; and the optimal solution is 1, 0.3, and 0.3 mmol/100 g for the polarization resistance, respectively. The polarization resistance R_p is inversely proportional to I_o, and the corrosion rate of the system can also be estimated by R_p [40]. In the optimal polarization resistance test (S9), X80 exhibited the lowest corrosion rate and the lowest corrosion degree, which is consistent with the results of the polarization curves and corrosion morphologies.

Table 5. Range analysis of the polarization results under orthogonal experiment

No.	$C(Cl^-)$	$C(SO_4^{2-})$	$C(HCO_3^-)$	Blank	E_o (V)	R_p ($\Omega/cm^{2\sim}$)	Corrosion rate (mm/a)
S9	1	1	1	1	0.50	55043	0.006
S4	1	2	2	2	0.45	9445.5	0.033
S2	1	3	3	3	0.58	2938.3	0.107
S8	2	1	2	3	0.48	6341.7	0.049
S5	2	2	3	1	0.53	7718.7	0.041
S7	2	3	1	2	0.58	2412.8	0.130
S3	3	1	3	2	0.47	11246	0.028
S1	3	2	1	3	0.59	2275.0	0.138
S6	3	3	2	1	0.54	11694	0.027
I_i	0.51	0.48	0.56	0.52	$\sum i = 1.55$		
II_i	0.53	0.52	0.49	0.50			
III_i	0.53	0.57	0.53	0.55			
R_i	0.03	0.08	0.07	0.05			
I_j	2.25E4	2.42E4	1.99E4	2.48E4		$\sum j = 6.66E4$	
II_j	5.49E3	6.48E3	9.16E3	7.70E3			
III_j	8.41E3	5.68E3	7.30E3	3.85E3			
R_j	1.70E4	1.85E4	1.26E4	2.10E4			
I_k	0.049	0.028	0.091	0.024			$\sum k = 0.168$
II_k	0.073	0.070	0.036	0.064			
III_k	0.064	0.088	0.058	0.098			
R_k	0.024	0.060	0.055	0.074			

3.2.2 Variance analysis of the polarization results

Table 6. Tests of between-subjects effects. Dependent Variable: Corrosion rate

Source	Type III sum of Squares	df	Mean Square	F	Sig.
Corrected Model	0.011[a]	6	0.002	0.460	0.805
Intercept	0.035	1	0.035	8.509	0.100
Cl^-	0.001	2	0.000	0.116	0.896
SO_4^{2-}	0.006	2	0.003	0.707	0.586
HCO_3^-	0.005	2	0.002	0.558	0.642
Error	0.008	2	0.004		
Total	0.054	9			
Corrected Total	0.019	8			

a. R Squared = 0.580 （Ajusted R Squared = -0.681）

The variance analysis of polarization results was performed by IBM SPSS statistics software [41-43]. After the data and results were edited into the data editor, the specific steps are as follows,

1. Analyse → General linear model → Univariate
2. Dependent variable box: selected E_o / I_o / R_p / Corrosion rate (only choose one)
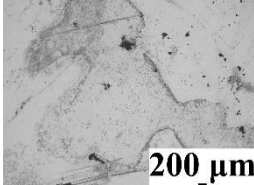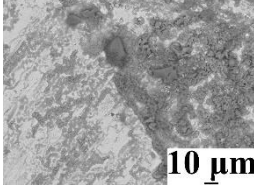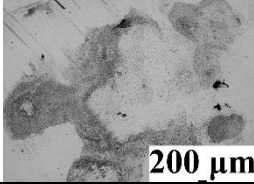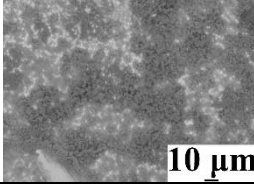
3. Fixed factors box: selected Cl^-, SO_4^{2-} and HCO_3^-

4. Model → Custom: selected

5. Model box: selected into the election of Cl^-, SO_4^{2-} and HCO_3^-; type: interaction, click OK

6. Post Hoc button → Post Hoc test for box: Selected Cl^-, SO_4^{2-} and HCO_3^-

7. SNK check box: selected, click OK

8. Click OK.

Because the *R* of the blank column is very large, the interaction type of the construction items was chosen in the Model tab. The mean difference is significant at a 0.05 level, which is a 95% confidence level [41, 42, 44, 45]. Here, the between-subject effects of the dependent variable corrosion rate is shown in Table 6 due to the consistent results. The results showed that the Cl^-, SO_4^{2-} and HCO_3^- factors were not statistically significant (P>0.05), which may be due to the level selection of experimental factors [41].

3.3 Macro- and micro- corrosion morphologies of X80 steel

The macro- and micro-corrosion morphologies of X80 steel in weak saline soils before descaling are shown in Table 7, including low magnification (×30, ×50) and high magnification (×1000). The sand particles attached to surface were removed by mechanical methods. The macro- and micro-corrosion morphologies show that the corrosion of X80 steel demonstrates slight local corrosion in the different saline soils. Moreover, the brown-yellow corrosion products (iron oxide) were generated on the surface of X80 steel [46, 47]. In addition, an opalescent microporous adhesive substance was attached to the surface of X80 steel in saline soils S1-S8, which may be the product of a Si-containing silica gel ($mSiO_2·nH_2O$) [48]. The results also exhibit acicular, flocculent clusters, and snow-like, rice granular corrosion products, which may be related to an acicular ferrite of the matrix steel [49, 50]. Among the soils, the corrosion of X80 steel in S9 is the weakest, which is identical with the results of the polarization curves.

Table 7. Macro- and micro- morphologies of X80 steel in saline soils under orthogonal experiment (before descaling).

No.	Macro morphologies	Micro morphologies	
		Low magnification(×30/×50)	High magnification (×1000)
X1		200 μm	10 μm
X2		200 μm	10 μm

No.	Macro morphologies	Micro morphologies	
X3		200 μm	10 μm
X4		200 μm	10 μm
X5		200 μm	10 μm
X6		200 μm	10 μm
X7		200 μm	10 μm
X8		200 μm	10 μm
X9		200 μm	10 μm
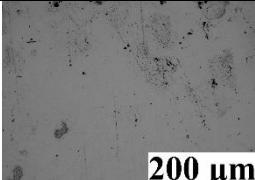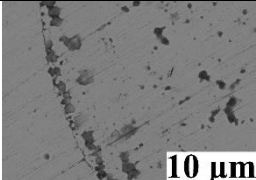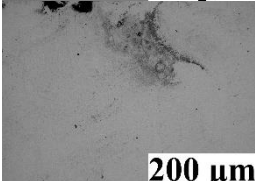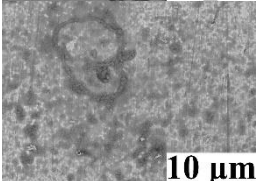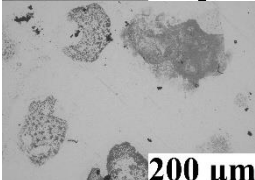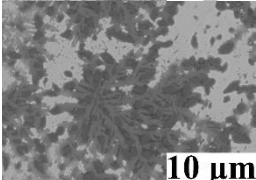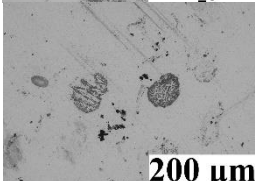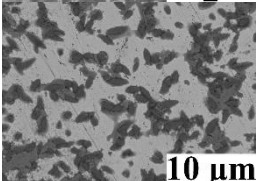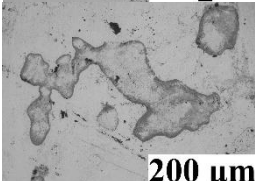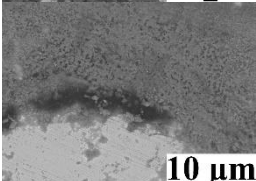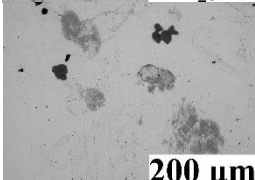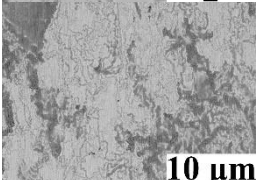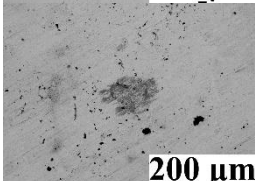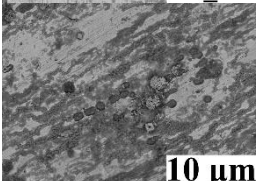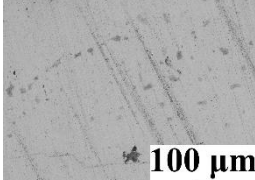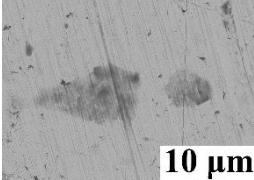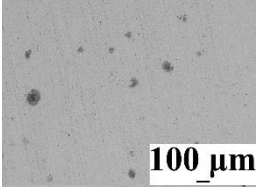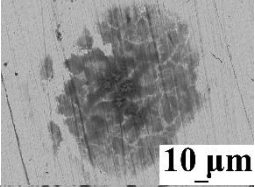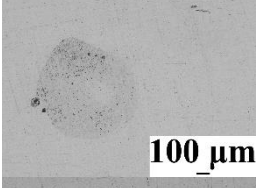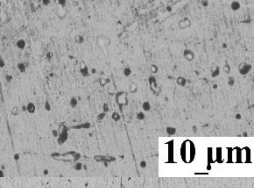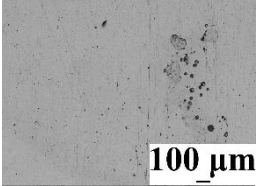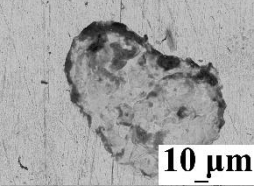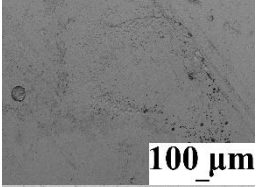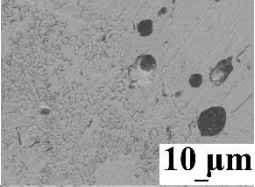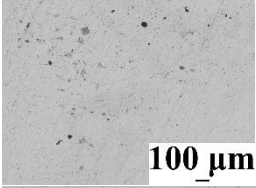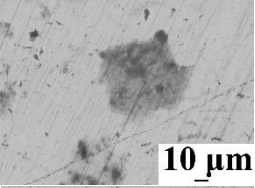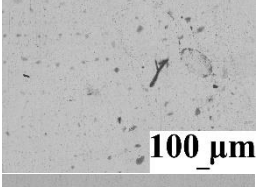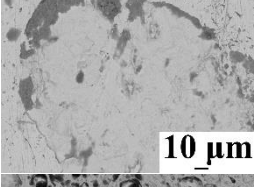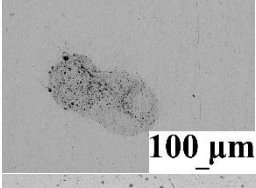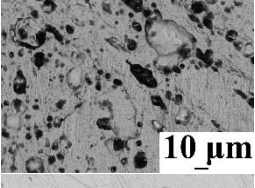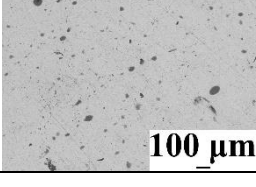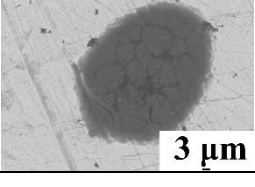
Table 8. Macro- and micro- morphologies of X80 steel in saline soils under orthogonal experiment (after descaling).

No.	Macro morphologies	Micro morphologies	
		Low magnification (×100)	High magnification(×1000/×2000)
X1		100 μm	10 μm

No.	Macro morphologies	Micro morphologies	
X2		100 μm	10 μm
X3		100 μm	10 μm
X4		100 μm	10 μm
X5		100 μm	10 μm
X6		100 μm	10 μm
X7		100 μm	10 μm
X8		100 μm	10 μm
X9		100 μm	3 μm

To further study the corrosion mechanism, the corrosion products of the X80 steels were removed by immersion in white vinegar for 2 h, and the macro- and micro-corrosion morphologies were also obtained, as shown in Table 8. The micro-topography includes low magnification (×100) and high magnification (×1000, ×2000) results. The macroscopic morphologies show that minor corrosion is demonstrated, i.e., mainly pitting corrosion, and no obvious corrosion pits are formed. Only some

darker metallic lustre areas appear on the surface. Therefore, there are more micro-corrosion pits on the surface of the X80 steel in S4 and S7 which is mainly pitting corrosion in a local area. In addition, the micro-cracks on the surface of X80 steel in S9 were probably caused by the alkaline environment of HCO_3^- [51, 52].

3.4 EDS analysis of the corrosion products

Figure 2 shows the EDS analysis results for the corrosion products in different saline soils. The corrosion products present acicular, flocculent clusters, snow-like and rice granular structures, which are mainly composed of Fe, O, C, and Si. The Fe/O ratios for the corrosion products on X80 steel are generally higher than the average Fe/O ratio (2.45) of iron oxide. Based on the fact that the content of O in the corrosion products is high, if the thickness of corrosion products layer is small, the Fe beneath the corrosion products could be detected by EDS, resulting a higher Fe/O ratio. Meanwhile, the detected Fe/O ratio could also reflect the portion of the corroded region to the test area, which is affected by the selection of test area. Fe/O ratio is a parameter measuring the volume of corrosion production in three-dimension (thickness and area proportion) reflecting corrosion rates of steels.

The Fe/O values (2.62, 3.28, 10.8, 3.66, and 5.39) in S5, S6, S1, S2 and S7, respectively, with a higher self-corrosion potential than that in S9 are generally lower than the corresponding values (23.14, 5.67, and 5.51) in S3, S8, and S4, respectively, with a lower self-corrosion potential than that in S9, which exhibits the smallest corrosivity. This result indicates that O in the corrosion products corresponds to a higher corrosion potential in S5, S6, S1, S2 and S7, which is higher than that in the other corrosion products. The corrosiveness of the corresponding saline sand is also stronger, which is consistent with the polarization curve results. A small amount of Si appears on the surface in the corrosion zone of X80 steel in different saline soils, which may be the compositional element of the milky white pore structure adhesive material ($mSiO_2 \cdot nH_2O$).

The cathodic process is the reduction of oxygen, which is the main process for corrosion control, and the anodic process is the dissolution of iron. The adsorption of Cl^- destroys the surface of the electrode and promote the occurrence of pitting corrosion. The presence of SO_4^{2-} and HCO_3^- in the liquid phase compete with Cl^- for adsorption, thus affecting the pitting process caused by Cl^-. This effect protects the diffusion of dissolved oxygen into the matrix and inhibited the effect of Cl^- to the corrosion [53]. The porous structure of the sandy soil also effects the reaction, causing the discontinuity of the reaction process.

In the saturated sandy soil (a typical porous medium), the oxygen in the pore liquid (in very small amount) may be competitively adsorbed by the micro-cathodes of X80 steel, which prolongs the diffusion path of oxygen [54]. Because limited amount of dissolved oxygen are available for the absorption of the steel micro-cathodes by diffusion, the depolarization effect of oxygen are weak. Therefore, the anodic reaction was inhibited, and the corrosion rate of X80 steel is small. In addition, Fe^{2+} generated by the anodic process might react with HCO_3^- in solution to form $FeCO_3$ (Eq. 7) due to the decrease in the depolarization effect of oxygen. In this status, Fe_2O_3 (Eq. 8) became the main corrosion product.
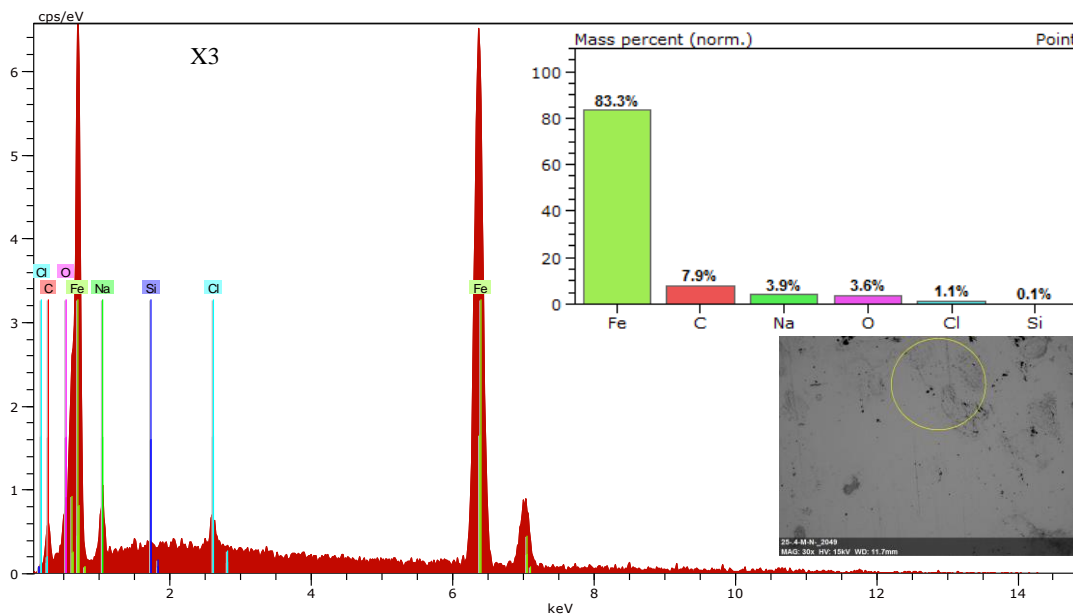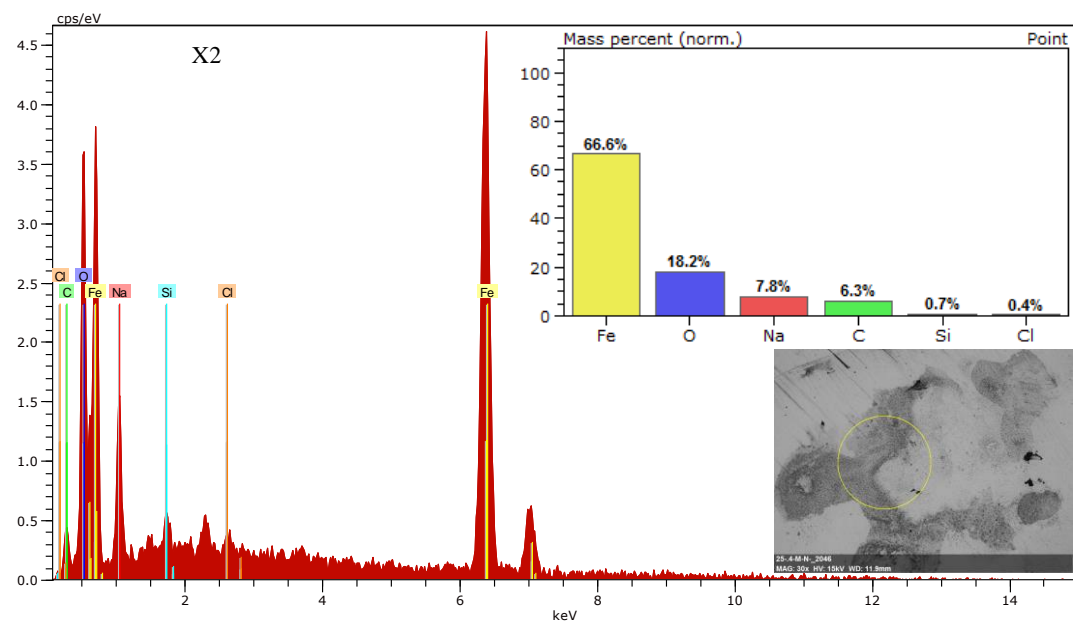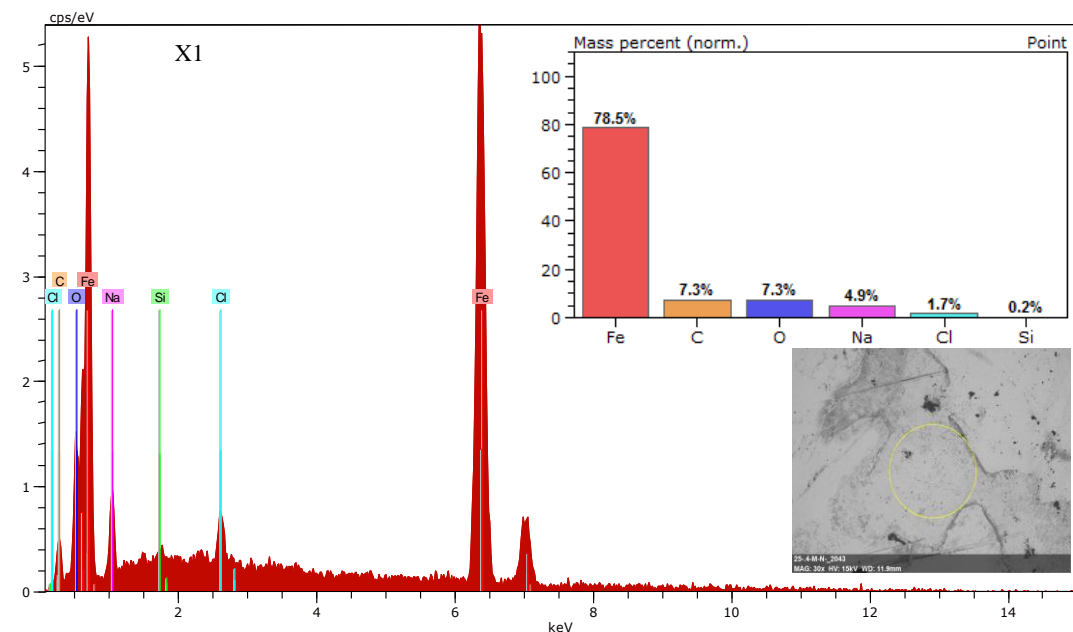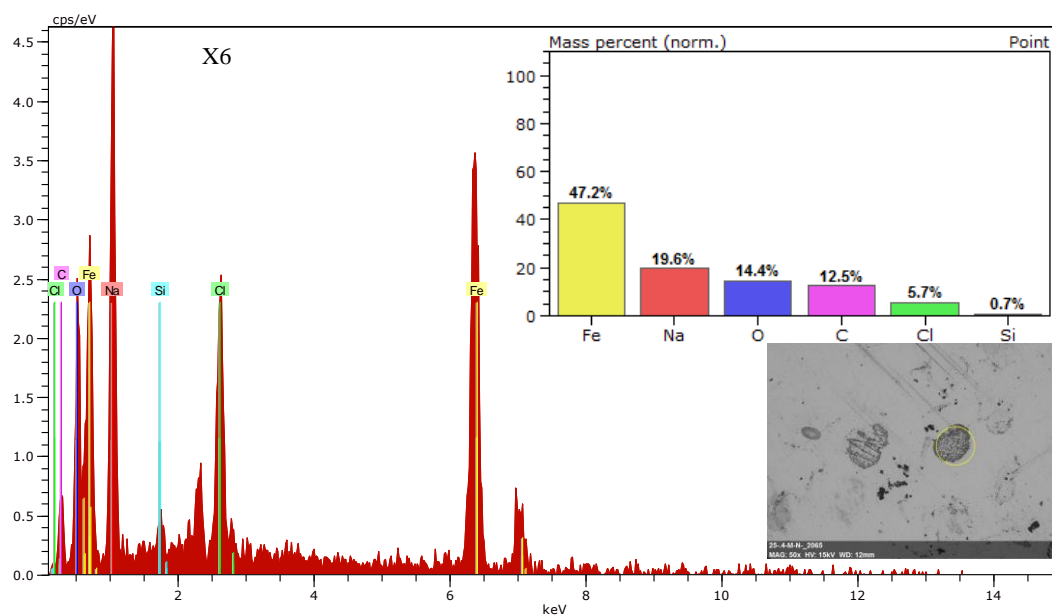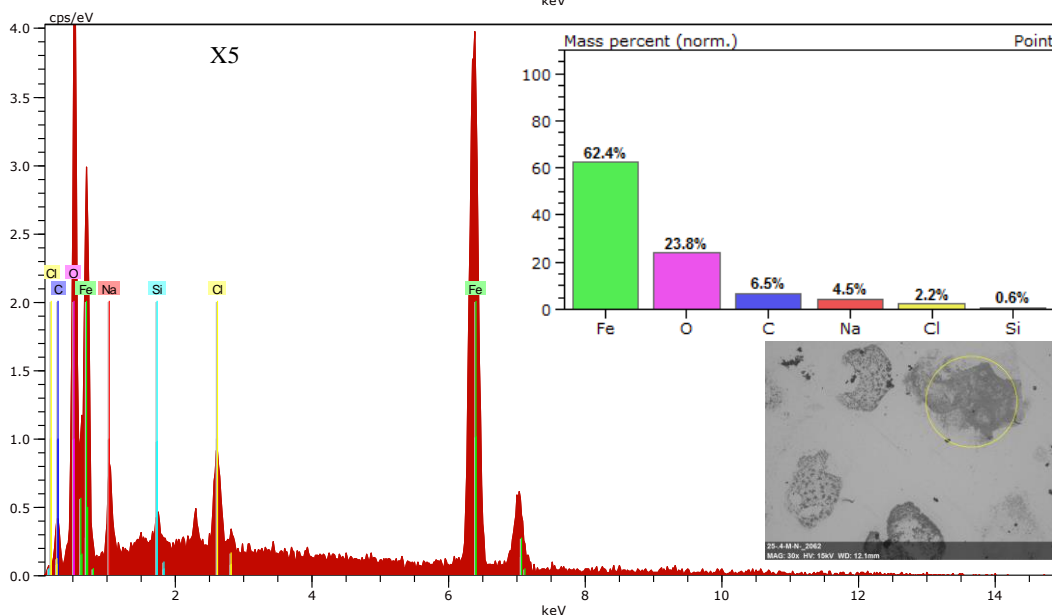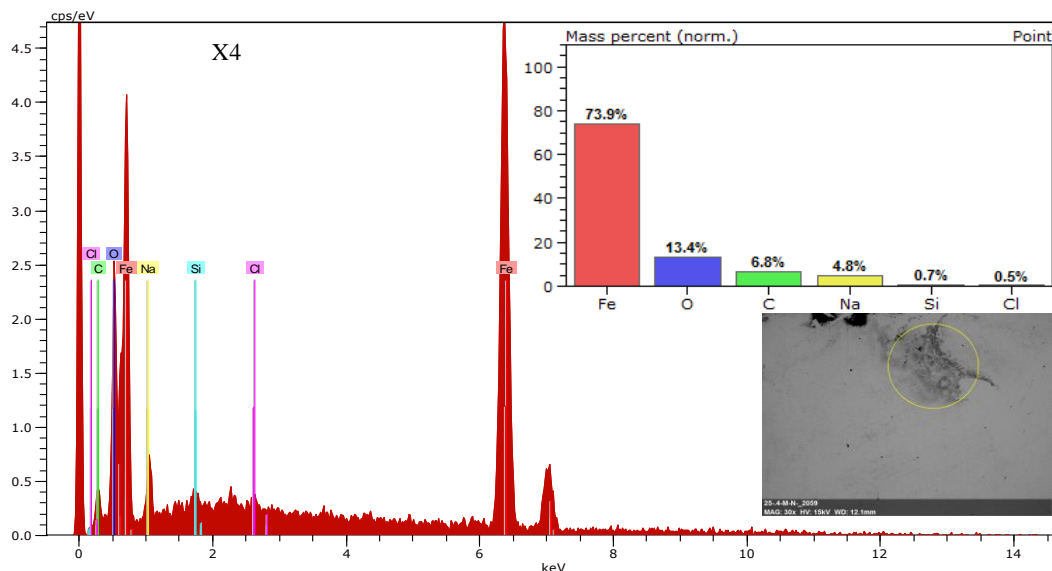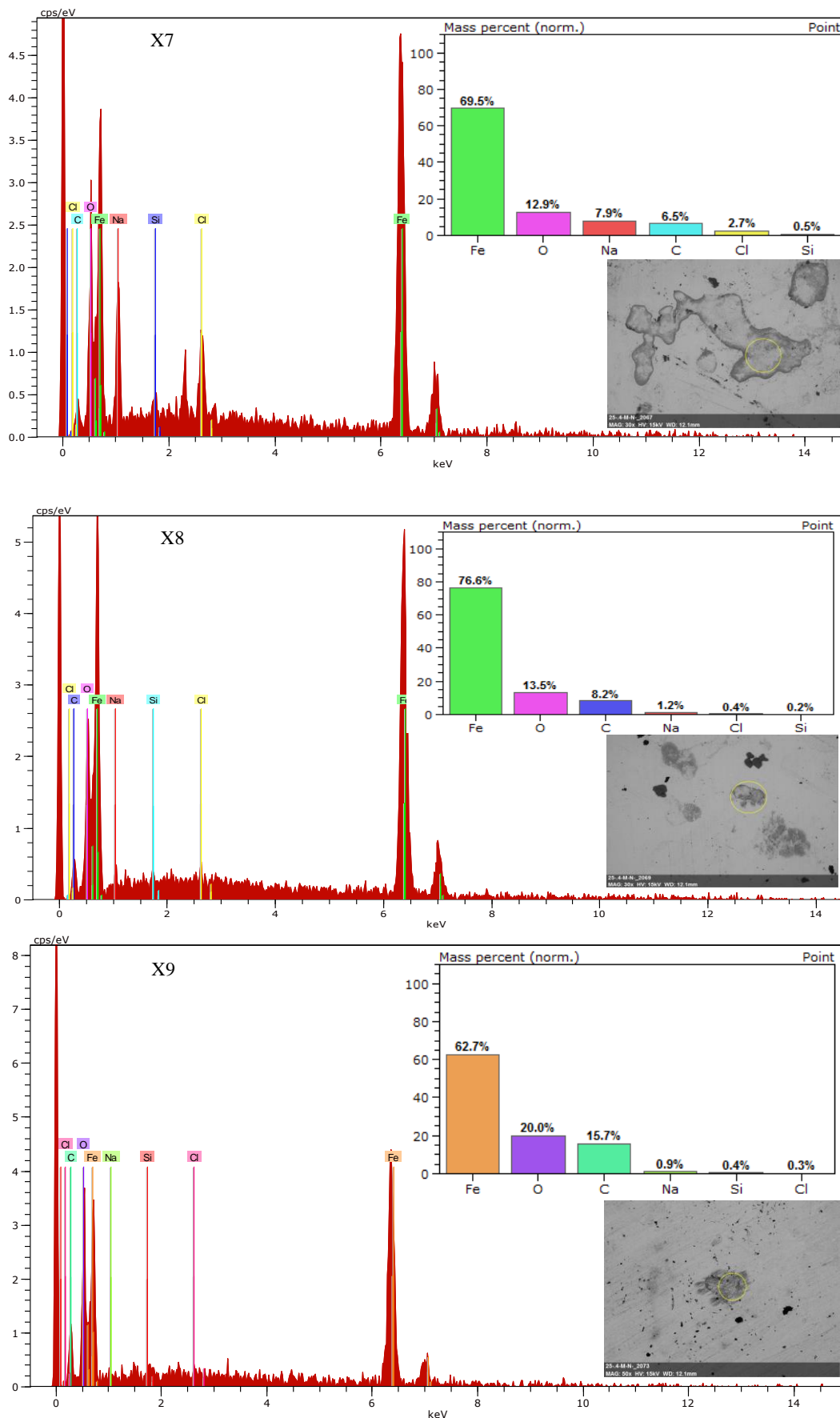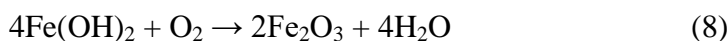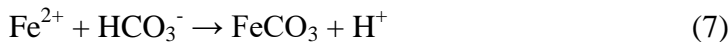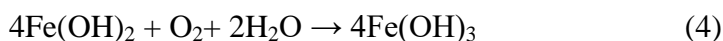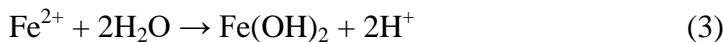
Figure 2. EDS results of surface corrosion products for X80 steel in saline soils

Generally, the protective effect of $FeCO_3$ was better than that of FeOOH, and the stability of Fe_2O_3 was also better. However, there is no significant passivity effect for X80 steel in sandy soil contaminated by Cl^-, SO_4^{2-} and HCO_3^- due to the influence of the porous media.

$$Fe - 2e \rightarrow Fe^{2+} \tag{1}$$
$$O_2 + 4H^+ + 4e \rightarrow 2H_2O \tag{2}$$
$$Fe^{2+} + 2H_2O \rightarrow Fe(OH)_2 + 2H^+ \tag{3}$$
$$4Fe(OH)_2 + O_2 + 2H_2O \rightarrow 4Fe(OH)_3 \tag{4}$$
$$2Fe(OH)_3 + Fe(OH)_2 \rightarrow Fe_3O_4 + 4H_2O \tag{5}$$
$$Fe(OH)_3 - H_2O \rightarrow FeOOH \tag{6}$$
$$Fe^{2+} + HCO_3^- \rightarrow FeCO_3 + H^+ \tag{7}$$
$$4Fe(OH)_2 + O_2 \rightarrow 2Fe_2O_3 + 4H_2O \tag{8}$$

4. CONCLUSIONS

An orthogonal experimental group of saline soils with soluble salt anions (Cl^-, SO_4^{2-} and HCO_3^-) was designed by orthogonal assistant and IBM SPSS Statistics 21 software. The initial dynamic potentiodynamic polarization of X80 embedded in different saline soils was tested using a three-electrode system. The statistical range and variance analysis of measurement data and an analysis of the corrosion morphologies and composition of X80 steel indicate the following:

1) The initial corrosion behaviour of X80 steel in S9 is the weakest, and the corrosion current density reaches 4.9E-7. The corrosive behaviour of X80 steel in different saline soils exhibits the following order: S9<S6<S3<S4<S5<S8<S2<S7<S1. SO_4^{2-} mainly affects the corrosion potential, and Cl^- and HCO_3^- mainly affect the corrosion current density.

2) The SO_4^{2-} is the most important factor affecting the initial corrosion behaviour of X80 steel. Cl^-, SO_4^{2-} and HCO_3^- were not statistically significant ($P > 0.05$), which may be due to the level selection of the experimental factors, and a further study is necessary. The optimal contents of Cl^-, SO_4^{2-} and HCO_3^- in sandy soil are 8, 2, and 0.3 mmol/100 g for E_o. The optimal contents are 1, 0.3, and 1 mmol/100 g for the corrosion rate, and the optimum contents are 1, 0.3, and 0.3 mmol/100 g for the R_p.

3) The corrosion of X80 steel in different saline soils exhibits a slight local corrosion and brown-yellow corrosion products (iron oxide) generated on the surface of the X80 steel. The opalescent microporous structure that adhered to the surface may be a Si-containing silica gel ($mSiO_2 \cdot nH_2O$). The corrosivity of saline soil S9 to X80 steel is the lowest.

4) The corrosion products are acicular, flocculent clusters, snow-like and rice granular, etc. The composition is mainly composed of Fe, O, C and Si. The corrosion products corresponding to S5, S6, S1, S2 and S7 with higher corrosion potentials present lower Fe/O ratios than those corresponding to the S3, S4 and S8 with lower corrosion potentials, indicating that the content of O in the corrosion products is high, and the corresponding corrosivity of saline sandy soil is also strong.

References

1. N.M. Lin, Q. Liu, J.J. Zou, D.L. Li, S. Yuan, Z.H. Wang and B. Tang, *RSC Adv.*, 7 (2017) 13517.
2. N.M. Lin, H.Y. Zhang, J.J. Zou, P.J. Han, Y. Ma and B. Tang, *Int. J. Electrochem. Sci.*, 10 (2015) 356.
3. W. Tian, W.H. Yu, N.M. Lin, J.J. Zou, J.W. Guo, H.Y. Zhang, P. Zhou, R.Z. Xie, Y. Ma, Z.X. Wang, X.F. Yao, P.J. Han, X.P. Liu and B. Tang, *Int. J. Electrochem. Sci.*, 10 (2015) 6057.
4. C.Q. Ren, N. Xian, X. Wang, L. Liu and Y.P. Zheng, *Corros. Eng., Sci. Technol.*, 47 (2013) 441.
5. M.H. Xu, W.H. Li, Y. Zhou, X.X. Yang, Z. Wang and Z. Li, *Int. J. Greenhouse Gas Control*, 51 (2016) 357.
6. W. Zhao, Y. Zou, K.J. Matsuda and Z.D. Zou, *Corros. Sci.*, 102 (2016) 455.
7. M. Zhu, C.W. Du, X.G. Li and Z.Y. Liu, *Mater. Corros.*, 66 (2015) 494.
8. M. Zhu and C.W. Du, *J. Mater. Eng. Perform.*, 26 (2016) 221.
9. F. Xie, D. Wang, C.X. Yu, Y. Zong and M. Wu, *Int. J. Electrochem. Sci.*, 12 (2017) 9565.
10. J.L. Zhou, X.G. Li, C.W. Du, Y.L. Li, T. Li and Y. Pan, *Acta Metall. Sinica*, 2010 (2010) 251.
11. J. Zhang, J. Liu, Q. Hu, F. Huang, Z.Y. Cheng and J.T. Guo, *Anti-Corros. Methods Mater.*, 62 (2015) 103.
12. D.H. Xia, S.B. Wu, Y. Zhu, Z.Q. Wang, Y.H. Sun, R.K. Zhu and J.L. Luo, *Electrochemistry*, 84 (2016) 238.
13. T.Q. Wu, J. Xu, M.C. Yan, C. Sun, C.K. Yu and W. Ke, *Corros. Sci.*, 83 (2014) 38.
14. T.Q. Wu, J. Xu, C. Sun, M.C. Yan, C.K. Yu and W. Ke, *Corros. Sci.*, 88 (2014) 291.
15. X.Z. Wang, Z.Y. Liu, X. Ge, X.L. Zhan, C.W. Du and X.G. Li, *Corrosion*, 70 (2014) 872.
16. X.H. Wang, C. Wang, X.H. Tang and Z.Z. Guo, *Int. J. Electrochem. Sci.*, 9 (2014) 8199.
17. D. Wang, F. Xie, M. Wu, D.X. Sun, X. Li and J.Y. Ju, *Int. J. Hydrogen Energy*, 42 (2017) 27206.
18. D. Wang, F. Xie, M. Wu, G.X. Liu, Y. Zong and X. Li, *Metall. Mater. Trans. A*, 48 (2017) 2999.
19. D. Wang, F. Xie, X. Li, X.F. Wang, J.Q. Liu and M. Wu, *corrrev*, 35 (2017) 445.
20. H.X. Wan, D.D. Song, Z.Y. Liu, C.W. Du, Z.P. Zeng, Z.G. Wang, D. Ding and X.G. Li, *Constr. Build. Mater.*, 154 (2017) 580.
21. H.X. Wan, D.D. Song, Z.Y. Liu, C.W. Du, Z.P. Zeng, X.J. Yang and X.G. Li, *J. Nat. Gas Sci. Eng.*, 38 (2017) 458.
22. S.X. Wang, D.X. Liu, N. Du, Q. Zhao and J.H. Xiao, *Adv. Mater. Sci. Eng.*, 2015 (2015) 1.
23. M.C. Yan, C. Sun, J. Xu and W. Ke, *Int. J. Electrochem. Sci.*, 10 (2015) 1762.
24. Z.Y. Liu, Q. Li, Z.Y. Cui, W. Wu, Z. Li, C.W. Du and X.G. Li, *Constr. Build. Mater.*, 148 (2017) 131.
25. L.M. Quej Ake, J. Marin Cruz and A. Contreras, *Anti-Corros. Methods Mater.*, 64 (2017) 61.
26. A.H.S. Bueno and J.A.C.P. Gomes, *J. Brazilian Soc. Mech. Sci. Eng.*, 31 (2009) 97.
27. L.B. Yu, M.C. Yan, J. Ma, M.H. Wu, Y. Shu, C. Sun, J. Xu, C.K. Yu and Y.C. Qin, *Acta Metall. Sinica*, 53 (2017) 1568.
28. C.O. Paul, E. Ahmed and A.M.A. Mohamed, *Int. J. Electrochem. Sci.*, 10 (2015) 10246.
29. K.S. Lim, N. Yahaya, N. Md Noor, S.N.F. Mior Mohd Tahir, J.K. Paik and Mohd H. Mohd, *Ships Offshore Struct.*, 12 (2017) 991.
30. W. Zhao, H. Zhang and Y. Zou, *Int. J. Electrochem. Sci.*, 12 (2017) 679.
31. Y.F. Wang, G.X. Cheng and Y. Li, *Corros. Sci.*, 111 (2016) 508.
32. H.R. Wang, C.W. Du, Z.Y. Liu, L.T. Wang and D. Ding, *Materials*, 10 (2017) 1.
33. Y. Wang, H.Y. Yu, Y. Cheng, H.T. Shan and D.B. Sun, *J. Univ. Sci. Technol. Beijing*, 35 (2013) 66.

34. H.Y. Tang, G.L. Song, C.N. Cao and H.C. Lin, *Corros. Sci. Prot. Technol.*, 7 (1995) 285.
35. H.Y. Tang, G.L. Song, C.N. Cao and H.C. Lin, *Corros. Sci. Prot. Technol.*, 8 (1996) 179.
36. H.Y. Tang, G.L. Song, C.N. Cao and H.C. Lin, *Corros. Sci. Prot. Technol.*, 8 (1996) 179.
37. Y.Y. Li and C.R. Hu, Experiment design and data processing Beijing: Chemical Industry Press, 2008.
38. S.R. Wang, Corrosion behavior and mechanism of X80 steel in Cl$^-$ and HCO$_3^-$ solution under the influence of alternating current (AC) Haidian District Beijing: University of Science and Technology Beijing, 2015.
39. L.S. Qu, X.G. Li, C.W. Du, S.Q. He and Z.Y. Liu, *J. Univ. Sci. Technol. Beijing*, 31 (2009) 1569.
40. J.Q. Zhang, Electrochemical Measurement Technology Beijing: Chemical Industry Press, 2010.
41. J. Gong, P.C. Shi and C.Y. Li, *Agric. Network Inf.*, 4 (2012) 31.
42. Z. Wang and L. Wei, *J. Math. Med.*, 27 (2014) 99.
43. X.Y. Yang, *Exp. Sci. Technol.*, 11 (2013) 41.
44. H. Qiu, G.Q. Jin, R.F. Jin and W.K. Zhao, *J. Chin. Integr. Med.*, 5 (2007) 101.
45. Z.J. Gao, S.L. Shi and Y. Li, *Prog. Mod. Biomed.*, 8 (2008) 2116.
46. N.M. Lin, P. Zhou, J.W. Guo, H.Y. Zhang, J.J. Zou, Y. Ma, P.J. Han and B. Tang, *Int. J. Electrochem. Sci.*, 10 (2015) 2694.
47. N.M. Lin, P. Zhou, Y.T. Wang, J.J. Zou, Y. Ma, Z.X. Wang, W. Tian, X.F. Yao and B. Tang, *Surf. Rev. Lett.*, 22 (2015) 1.
48. https://www.bmlink.com/zhcilcon/news/986025.html
49. S.X. Wang, D.X. Liu, N. Du, Q. Zhao and J.H. Xiao, *Int. J. Electrochem. Sci.*, 11 (2016) 2534.
50. S.X. Wang, D.X. Liu, N. Du, Q. Zhao and J.H. Xiao, *Int. J. Electrochem. Sci.*, 11 (2016) 8797.
51. A. Torres Islas and J.G. Gonzalez Rodriguez, *Int. J. Electrochem. Sci.*, 4 (2009) 640.
52. J.D. Kang, W.Y. Zheng, D. Bibby, B.S. Amirkhiz and J. Li, *J. Mater. Eng. Perform.*, 25 (2016) 3546.
53. W.P. Zhang and X.Y. Li, *Yunnan Chem. Technol.*, 40 (2013) 8.
54. S.X. Wang, D.X. Liu, N. Du, Q. Zhao, S.Y. Liu and J.H. Xiao, *Int. J. Electrochem. Sci.*, 10 (2015) 4393